Landslides (2021) 18:2247–2263
DOI 10.1007/s10346-021-01635-3
Received: 23 September 2020
Accepted: 29 January 2021
Published online: 8February 2021

Nicola Cenni · Simone Fiaschi · Massimo Fabris

Integrated use of archival aerial photogrammetry, GNSS, and InSAR data for the monitoring of the Patigno landslide (Northern Apennines, Italy)

Abstract The morphological changes of unstable areas can be identified using different methodologies that allow repeated surveys over time. The integration between the data obtained from different remote sensing and ground-based techniques, characterized by different coverage, resolution, and precision, allows to describe the kinematic motion of landslides with high accuracy and details. The aim of this work is to monitor the displacements of the Patigno landslide, a deep-seated gravitational slope deformation located in the Northern Apennines (Zeri, Massa Carrara, Italy), using archival aerial photogrammetry (1975–2010), continuous GNSS observations (2004–2018), and multi-temporal InSAR data (2015–2019). The results obtained adopting the different techniques were cross-validated and integrated in order to better explain the kinematics of the landslides: the GNSS data analysis shows horizontal movements of about 43 mm/yr in the S-E direction and vertical deformations of 6.5 mm/yr, in agreement with the average displacement rates obtained from photogrammetry and InSAR processing. The analysis of multi-temporal aerial photogrammetric images allowed us to observe three sectors of the landslide body characterized by different velocities rates and planimetric directions, in agreement with the LOS InSAR displacement field. Furthermore, the correlation between the rainfall distribution and the GNSS time series shows an acceleration of the sliding movements after about 3–4 months of a strong rainfall period. This integrated approach allowed us to overcome the limitations of each technique and to provide a 44-year long monitoring of the Patigno landslide. We also show that a synergic use of ground-based and remote sensing methodologies can provide useful information for the planning of more effective landslide risk mitigation strategies.

Keywords Landslides · Multi-technique monitoring · Aerial photogrammetry · GNSS · InSAR · Northern Apennines (Italy)

Introduction

Landslides are very frequent geological hazards in many regions of the world. In the Italian peninsula, for example, about 620,000 landslides have been mapped and reported on the I.F.F.I. catalogue (Inventario Fenomeni Franosi Italia, ISPRA 2020). Slope instabilities can be triggered by both natural (e.g., intense rainfalls and/or seismic events) or anthropogenic (e.g., poor urban planning and/or deforestation) factors, and they can cause damage to buildings and infrastructures and have severe socio-economic impacts.

The monitoring of the spatial and temporal evolution of landslides is therefore crucial in order to evaluate the hazard, manage the risk, and define prevention and mitigation strategies. Different techniques and tools are available for monitoring the evolution of a landslide. Several researchers (e.g., Feng et al. 2020; Kean et al. 2015; Manconi et al. 2016; Yan et al. 2020; Liu et al. 2018) have proposed methodologies to understand the motion and deformation characteristics of the landslides based on the seismic and acoustics signals generated by the movements of the landslides. These studies analyzed the signals acquired by networks of accelerometers and microphones located near or in the landslide area (Feng et al. 2020; Liu et al. 2018). In other cases, in the absence of on-site monitoring networks, the waveforms acquire from regional or local seismic networks was analyzed in order to detect, locate, and estimate the volume of rockslides (Manconi et al. 2016). The ground-based methods such as the conventional wire extensometers (e.g., Corominas et al. 2000), automated total stations (e.g., Frigerio et al. 2014), inclinometers (e.g., Zhang et al. 2018), leveling campaigns (e.g., Cotecchia et al. 1995; Colesanti et al. 2003), and continuous GNSS or non-permanent sites (e.g., Pesci et al. 2004; Baldi et al. 2008; Cina and Piras 2015; Glansch et al. 2009) can provide pointwise and accurate information about the landslide movements. Other techniques, such as the digital aerial and unmanned aerial vehicle (UAV) photogrammetry (e.g., Achilli et al. 2015; Fabris and Pesci 2005, Fabris 2019), terrestrial and airborne laser scanning (TLS, ALS) (e.g., Fanti et al. 2013; Fabris et al. 2010; Frodella et al. 2016), and radiometric satellite images and Interferometric Synthetic Aperture Radar (InSAR) techniques (Calò et al. 2014; Del Soldato et al. 2019, Komac et al. 2015), allow the monitoring of large areas with high point density. Repeated surveys with ground-based approaches (extensometers, inclinometers, leveling, topographic measurements, and GNSS) allow the estimation of extents and rates of deformations in a relatively low number of benchmarks only in accessible sectors of the landslide. The observations acquired, for example, from GNSS sites can often provide important information on the temporal evolution of the phenomenon with high accuracy values (less than 10 mm). However, the sustainability of a ground-based monitoring is often hampered by budget and technical constraints, such as the extent of the investigated area and the high management costs of the installed instrumentation, which limit the feasibility of long-term studies (Calò et al. 2014). On the other hand, the "remote" techniques (InSAR, radiometric satellite images, photogrammetry, and laser scanning) allow to measure movements over large areas but with some limitations given by low precision (e.g., for archival aerial photogrammetry), lack of reliable reflective surfaces in non-urbanized areas (e.g., for InSAR), and the use of a local reference system for the estimation of displacements. In particular, aerial photogrammetric surveys allow the analysis of the landslide movements for long periods covering large areas at medium to high resolutions, but with accuracies up to few tens of centimeters at most, depending mainly on the camera-object distance and the images resolution.

The InSAR approach has been used for Earth observation purposes since the 1990s of the last century and provides measurements of surface motions at high spatial resolution, commonly between 3 and 100 m, and with high accuracies, in the order of 1–2 mm/yr. The movements measured by the InSAR technique are also limited to the line of sight (LOS) of the satellite and only if both acquisition geometries (i.e., ascending and descending orbits) are available it is possible to obtain the East-West and Vertical components of the movement. However, the "remote" techniques

have often the advantage to be less demanding in terms of costs and technical resources in respect to the ground-based methods.

The challenges of landslide monitoring can be overcome only through the use of an integrate approach in which the advantages of each single technique compensate the defects of the others. The accuracy of these monitoring techniques is also important to define the limits of the warning systems that could be developed and used to monitor the landslide area. The aim of ground and remote sensing approaches should be to estimate the spatio-temporal evolution of the movements on the landslide area in order to better define more effective early-warning systems and reduce the landslide risk. The overlapping between the observation periods of the adopted techniques should be a necessary requirement for the use of an integrated monitoring approach. This condition is usually satisfied when the landslide monitoring is supported by a financed project. In the cases where this condition is not satisfied, the integrated monitoring is carried out using the data acquired for other aims, which do not guarantee the necessary overlapping periods.

This paper focuses on the monitoring of the slope movements of the Patigno landslide (Tuscany Region, Northern Apennines, Italy) (Fig. 1) using archival aerial photogrammetric surveys, GNSS observations, and multi-temporal InSAR data. These observations are not completely overlapped because they have been acquired for different aims respect the landslide monitoring. The integrated approach allowed us to observe the evolution of the landslide occurred in the last 44 years and to identify the area where the kinematic pattern has changed. These could be the areas more at risk, where mitigation strategies should be adopted in order to prevent or reduce the possible consequences of a destructive slope activation.

Background

The Patigno landslide is located in the north-western sector of the Lunigiana graben, a part of the western side of the Northern Apennines where three Italian political Regions (Liguria, Emilia Romagna, and Tuscany) meet (Fig. 1a). The study area extends in the municipality of Zeri (Massa Carrara province, Tuscany Region) for about 2500 m from N-W to S-E with an elevation between 1000 and 550 m a.s.l. The Patigno hamlet is located on the homonymous landslide, characterized by an average inclination of about 10° and collocated in the hydrographic basin of the Gordana river (Federici et al. 2002). The part of Northern Apennines encompassing the landslide area is characterized, from the geological point of view, by three different tectonic units: the Ligurian (internal and external), Subligurian, and Tuscan Units (Bortolotti et al. 2001; Carmignani et al. 2001; Di Naccio et al. 2013). The Tuscan domain, mainly constituted by the Macigno Formation, flysch, and sandstones, is tectonically overlapped by the Subligurian domain here represented by the Canetolo Unit. The Canetolo Unit is characterized primarily by argillaceous and arenaceous rocks, Groppo del Vescovo limestone, and Ponte Bratica sandstone (Federici et al.

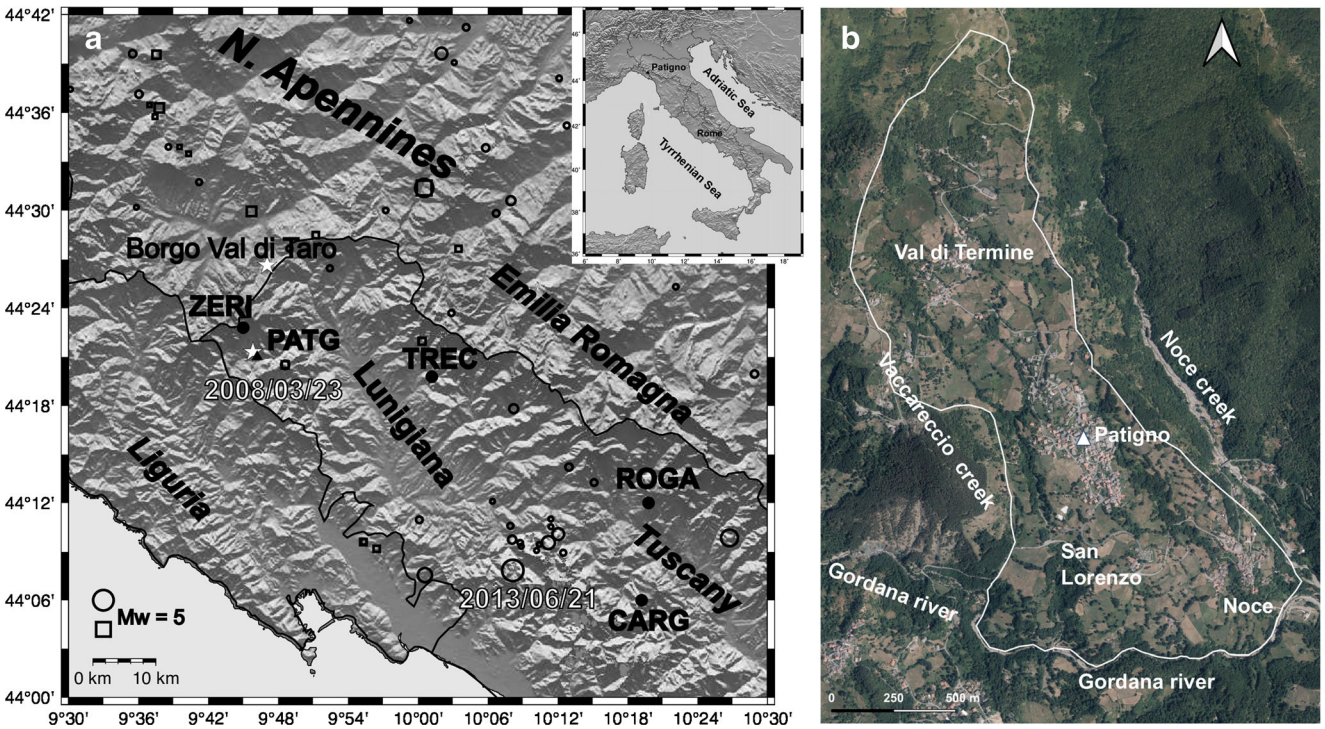

Fig. 1 Map of the Patigno study area. **a** Location of the Patigno landslide in the Northern sector of the Italian peninsula. Position of the other four CGNSS sites involved in the monitoring of the landslide: CARG (Careggine), ROGA (San Romano in Garfagnana), TREC (Treschietto-Bagnone), and ZERI (Passo dei due Santi, Zeri). The white stars indicate the positions of Patigno and Borgo Val di Taro pluviometers. Circles and squares show the positions of the seismic events with magnitude greater than 3.5 occurred from the 1975 and reported respectively on the Italian Seismological Instrumental and Parametric Data-base (ISIDe 2007) and on the Parametric Catalogue of Italian Earthquake (CPTI15 v 2.0, Rovida et al. 2020). The dimension of the symbols is proportional to the moment magnitude (Mw) reported on the respective catalogues. **b** Sketch map of the Patigno landslide: white line shows the boundaries of the landslide and the white triangle indicate the position of the continuous GNSS station. The position of Patigno village, Noce, San Lorenzo, and Val di Termine hamlets are also shown

2002). The uppermost tectonic unit is the Ligurian domain constituted by the Ottone S. Stefano Unit. The substrate of the landslide area is characterized by the Canetolo Unit (Federici et al. 2002) that crops out in the eastern side of the area, and it is separated from the Ottone S. Stefano Unit by a NW-SEthrust belt structure, while the non-metamorphic Tuscany Unit crops out in the eastern side of the area (Federici et al. 2000, 2002; Raiti et al. 2006). The Vaccareccia and Noce creeks flow near the western and eastern borders of the landslide area (Fig. 1b), and the Gordana river causes significant erosion of the landslide toe.

Seismic events can represent a triggering factor for the activation and/or sliding acceleration of landslides, as suggested by some authors (e.g., Dreyfus et al. 2013; Refice and Campolongo 2002; Umar et al. 2014). The earthquakes occurred in the Lunigiana graben area and in the western side of the Northern Apennines since 1 January 1975 are shown in Fig. 1a, as reported in the Italian Seismological Instrumental and Parametric Data-Base (ISIDe 2007) and in the Parametric Catalogue of Italian Earthquake (CPTI15 v 2.0, Rovida et al. 2020). The seismicity in the study area is characterized by low-moderate events. It can be noted that in the period considered in this study, the landslide area and its surroundings (with distances less than 10 km from the Patigno landslide) were interested only by one earthquake occurred in 26 March 2008, with a moment magnitude equal to 4.0 (ISIDe 2007, Rovida et al. 2020). This event was located at a depth of about 72 km (ISIDe 2007; Rovida et al. 2020), and it was only registered by the instruments without documented damages and/or alert from the population. The relatively low magnitude of the earthquake and the high depth of the hypocenter could suggest that this event did not have a significant impact on the re-activation or sliding acceleration of the landslide.

Previous studies (Federici et al. 2000, 2002; Stucchi et al. 2014) used high-resolution refraction and reflection seismic surveys and boreholes to define the geometry of the landslide body. The interpretation of the boreholes and seismic data indicates an undisturbed bedrock at a depth of about 40–50 m, overlaid by an intermediate layer of densely fractured argillites and limestone rocks of the Canetolo Unit with a thickness of about 30 m, and a shallower layer of unconsolidated landslide material (sands, gravels and boulders). The presence of fresh scarps, surfaces with counter/gentle slope, and tension cracks is the geomorphological evidence that the landslide is still active. Previous geological and geophysical surveys (Federici et al. 2002; Raiti et al. 2006) indicate that the landslide began as a single movement and dismantled into several slides and flows. Federici et al. (2002) have monitored the landslide movements for 6 months (June–December 1999) using boreholes equipped with inclinometers. The instrument located in the lower sector of the landslide observed a S-E displacement greater than 35 mm (about 70 mm/yr) at a depth of 12–19 m. The inclinometer located in the Patigno hamlet, the central sector of the landslide, detected a S-E movement of 6–7 mm (12–14 mm/yr) at less than 12 m of depth. Baldi et al. (2008), analyzing the GNSS observations acquired by a continuous station located in the Patigno village, measured a strong horizontal movement (E150° S direction) of 35 mm/yr and a mean vertical velocity of about −4 mm/yr: this result is in good agreement with the displacements measured by Raiti et al. (2006) using inclinometers. The photogrammetric analysis has highlighted some localized slip episodes and a slow downslope movement of the landslide with a consequential height decrease in the upper part of the slope and a height increase in the lower sector. Del Soldato et al. (2019) have investigated 25 years of InSAR observations (from 1992 to 2018) in order to identify the damage on structures and infrastructures due to the Patigno landslide movements. In particular, the authors have measured and found increasing velocities from N-W to S-E, with rates from −15 mm/yr in the Northern sector of the village to about −50 mm/yr in the San Lorenzo hamlet.

Available datasets and data analysis

Archival aerial photogrammetric surveys

For this study, we analyzed several images obtained from 5 aerial photogrammetric surveys carried out in 1975, 1987, 2004, 2010, and 2013, available from Tuscany Region (Table 1). To perform the digital processing, the images of the 1975, 1987, and 2004 surveys were rasterized using the Wehrli Raster Master RM2 photogrammetric scanner with resolution of 12 μm, which allowed us to obtain a ground sample distance (GSD) ranging from 16 to 36 cm. The last two surveys of 2010 and 2013 were acquired with the Vexcel UltraCam Xp digital metric camera which provides GSD respectively of 15 cm and 40 cm. The images of 1987, 2004, 2010, and 2013 are characterized by a poor visibility on the ground due to the vegetation and urbanization cover, while the images of 1975 show only few obstacles over the whole landslide area.

The common reference system for the co-registration of the 5 multi-temporal datasets was obtained by identifying homologous artificial points on the images series, supposed stable, and located outside to the landslide area. The coordinates of these points, used like ground control points (GCPs), were measured on the Carta Tecnica Regionale (CTR) at scale 1:5000 obtained from the same aerial photogrammetric survey of 1975 used in this study (Baldi et al. 2008). The coordinates of 60 GCPs (mainly corners of buildings/roofs) were obtained in the UTM, zone 32, reference system. Each aerial photogrammetric survey was processed with the SOCET SET (SoftCopy Exploitation Tool Set) software; the internal orientation of the images was carried out with the available camera calibration data, while the external orientation was performed by measuring well-defined homologous tie points together with the GCPs for images/block connection and model adjustment. The relative co-registration between the multitemporal stereoscopic models, assuming the first as reference, was verified by manually measuring, using stereoscopic devices, natural and/or artificial well-defined points located outside the landslide area (Table 2).

Subsequently, starting from each stereoscopic 3D model, a digital elevation model (DEM) was extracted automatically with a grid size of 5 m on the area that includes the landslide and the surrounding portions. Automatic correlation procedures in corresponding portions of the images were applied by means of an algorithm based on the comparison between the gray/color level distribution in homologous areas of the images.

Since the 1975 images present good visibility over the whole landslide, a digital terrain model (DTM) was obtained adapting the contour level to the real terrain morphology by means of the stereoscopic devices: elevation of the points over objects in the ground (trees and buildings) was corrected by the operator based on the 3D stereoscopic viewing. The comparison between the DEMs can generally be used to measure the variations of land

Table 1 Main characteristics of the aerial photogrammetric surveys used in the multi-temporal analysis

Survey	Strips	Images	Format (cm)	Scale	Calibrated focal length (mm)	GSD (cm)
1975	2	7	23×23	113,000	152.67	16
1987	2	8	23×23	113,000	152.22	16
2004	I	3	23×23	130,000	153.64	36
2010	3	18	6.79×l0.39 (11310×l7310 pixel)	110,000	100.50	15
2013	2	8	6.79×l0.39 (11310×l7310 pixel)	130,000	100.50	40

The GSD is the ground sample distance

mass: however, due to co-registration errors, the vegetative coverage, and the type of deformation in progress (sliding of the masses along the slope), in this case, it is not possible to obtain acceptable results with this method (Baldi et al. 2008). To overcome this limitation, and to identify movements inside the unstable portion, we manually measured homologous points inside the landslide area in the multi-temporal dataset starting from the stereoscopic models. In each model, we identified and measured 165 multi-temporal well-visible points (still mainly corners of buildings), and we obtained the 3D displacement vectors in five periods (1975–1987, 1987–2004, 1987–2010, 2004–2010, and 2010–2013) by comparing the coordinates of such points. Due to the vegetation cover, the points were measured almost exclusively in the built-up areas of the Patigno, Noce, and Val di Termine villages (Fig. 1b) and, for a limited extent, on isolated buildings. Due to the different precision of the photogrammetric data (Tables 1 and 2), the generation of displacement vectors was more reliable for the 1975–1987 and 1987–2010 comparisons (Fig. 2).

To get further insights about the displacement fields shown in Fig. 2, we have computed the interpolated velocity field and the related horizontal strain rate tensor within a regular grid. We have adopted the method suggested by several authors (e.g., Cenni et al. 2012; Pesci et al. 2009; Teza et al. 2008) in order to estimate the interpolated velocity field and the strain rate pattern starting from an irregular space distribution of horizontal velocities observed on continuous GNSS (CGNSS) and/or non-permanent sites. This procedure has been developed using a weighted least square method that, starting from the horizontal velocity values, solves the two horizontal velocity components and the four velocity gradients using six parameters (Cenni et al. 2012, and reference therein). The weights are estimated by scaling the variance associated to the velocity values with an exponential scaling function e^(d_{ik}/D), where D is the distance decay factor, a user-dependent parameter, and d_{ik} is the distance between the k_{th} photogrammetric ground point and the i_{th} node of the grid. As suggested by Cenni et al. (2012), we have also introduced two geometric criteria: (i) the interpolated values are taken as acceptable only when at least three ground points are located at a distance lower than D from the grid-point taken into account, and (ii) such sites are uniformly distributed in the surrounding region (one in each of 120° angular sectors).

GNSS dataset

In January 2004, a continuous GNSS station (PATG, Fig. 1b) was installed in the Zeri town hall located on the Northern sector of the Patigno hamlet. The double frequency observations acquired from 1 January 2004 to 31 December 2018 were processed using two different software: GAMIT version 10.7 (Herring et al. 2018) and RTKLib version 2.4.2 (Takasu 2013). The PATG data were processed using GAMIT software together with observations collected from four other CGNSS stations (CARG, ROGA, TREC, and ZERI) located on stable rock outcrops or buildings on the Tuscany sector of the Northern Apennines near the Patigno landslide (Fig. 1a). Moreover, we have adopted the double difference static positioning mode of RTKLib to estimate the position of the Patigno CGNSS site. This approach requires defining a reference station whose coordinates are fixed during the estimation procedure. We have developed two different processing in order to estimate how the distance from the reference station and the length of observation can influence the estimation of the position and the corresponding velocity values. The first reference site selected is the permanent station located closest to the landslide: the ZERI station on the

Table 2 Average and standard deviation of the comparison between the coordinates of check points located outside to the landslide area that provides the order of magnitude of the relative co-registration between the subsequent photogrammetric models

Comparison		1975–1987	1987–2004	2004–2010	2010–2013	1987–2010
Number of points		40	25	32	28	26
GSD (cm)		16–16	16–36	36–15	15–40	16–15
Average (cm)	East	3	2	8	−12	7
	North	4	−10	10	10	−4
	Vertical	3	−11	−7	12	5
Standard deviation (cm)	East	13	23	22	31	14
	North	14	21	28	34	12
	Vertical	13	24	20	32	15

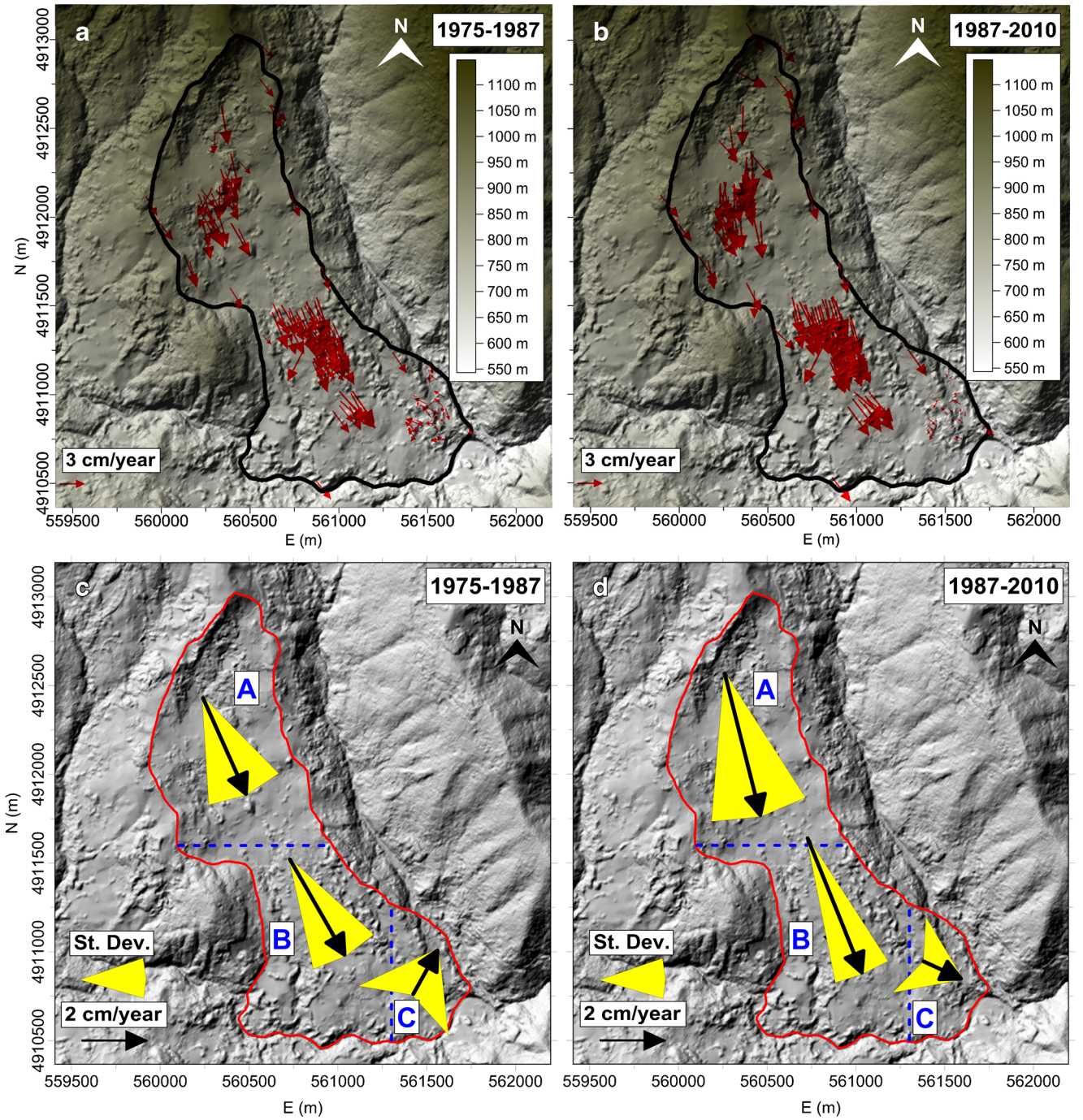

Fig. 2 Velocities and horizontal direction averaged on the 2010 DSM. **a** Velocities obtained comparing the 1975 and 1987 aerial photogrammetric data. **b** Velocities computed comparing the 1987 and 2010 surveys. The measured vectors are denser in built-up areas of Val di Termine, Patigno, San Lorenzo, and Noce. **c** 1975–1987 average velocities in the A, B, and C sectors obtained averaging the rates of the points inside to the 3 sectors; standard deviations related to the directions of the resulting velocities are also reported. **d** 1987–2010 average velocities and related standard deviations

Passo due Santi in the municipality of Zeri (the distance between PATG and ZERI is about 4 km). The selection of the second reference site was performed by comparing the observation period of the PATG station with those of the sites located at a distance less than about 55 km. The selected site, ROGA, presents the longest overlapping observation period of about 15 years (Table 3). The raw observations acquired with a 30-s sampling rate of the five CGNSS sites have been processed with the GAMIT software using the parameterizations described in Baldi et al. (2008). The coordinates of the ROGA reference site have been calculated using a regional network adopting the approach described in Cenni et al. (2012, 2013, 2015) and updated to 31 December 2018. The daily time-series of the North, East, and Vertical geographic position components of the five sites included in the network have been

analyzed using the procedure described in Cenni et al. (2012, 2013, 2015). The RTKLib library has provided other daily time series of the Patigno station that were analyzed using the same method adopted for the GAMIT time series. The obtained velocities and the root mean square (RMS) values are reported in Table 3, where PAT1 and PAT2 correspond to the Patigno RTKLib process with ROGA and ZERI as reference sites respectively. These velocities were obtained using a weighted least square method supposing a white noise model in the time series. Several authors (Mao et al. 1999; Wang et al. 2012; Bos et al. 2013) have demonstrated that if a white noise model is implemented, the uncertainties associated with the parameters may be underestimated with a factor from 5 to 11. We have taken into account this underestimation and the impact of some processing biases, as described in He et al. (2017), multiplying by a factor 15 the uncertainties estimated with white noise. The resulting horizontal and vertical velocities of the sites included in the GAMIT network (CARG, TREC, ZERI) are lower than 1 mm/yr (Table 3). These values represent the relative velocities between these sites and the ROGA reference station used to translate the daily solution into the same local reference frame. Cenni et al. (2012, 2013 and 2015) analyzing the same CGNSS stations in a regional network (about 700 CGNSS stations located on the Italian peninsula and surrounding areas) obtained relative velocities in agreement with the values reported in Table 3. This agreement suggests that the use of ROGA as a reference site has not introduced significant deformations in this network.

Rainfall dataset

The rainfall data acquired from two stations, the first located in the landslide area (Patigno site) and the second in the Borgo Val di Taro village (Fig. 1), have been used to estimate the temporal evolution of the rainfall in the landslide area. Rainfall records from 1 January 2009 to 31 May 2020 available for the Patigno site have been downloaded from the Tuscany Region's Settore Idrologico e Geologico Regionale (SIR) data sharing service (http://www.sir.toscana.it/, in Italian language only). The Patigno rainfall observation period overlaps only partially with the GNSS data (from 1 January 2004 to 31 December 2018); to increase the overlap between the GNSS and the rainfall data, we have analyzed also the daily rainfall data (from 31 October 2002 to 31 May 2020) obtained from the Borgo Val di Taro village station, located about 15 km from the landslide area, which completely overlap with both the GNSS station and the Patigno rainfall time series (data available from the ArpaE-SIM data sharing service, https://simc.arpae.it/dext3r, in Italian language only). The two datasets have a Person's correlation coefficient of about 0.7 and a vanishing time lag that indicates a good agreement between the data (Fig. 3a). This suggests that it is possible to use the Borgo Val di Taro rainfall data as representative of the rainfall distribution on the Lunigiana area, where the landslide is located.

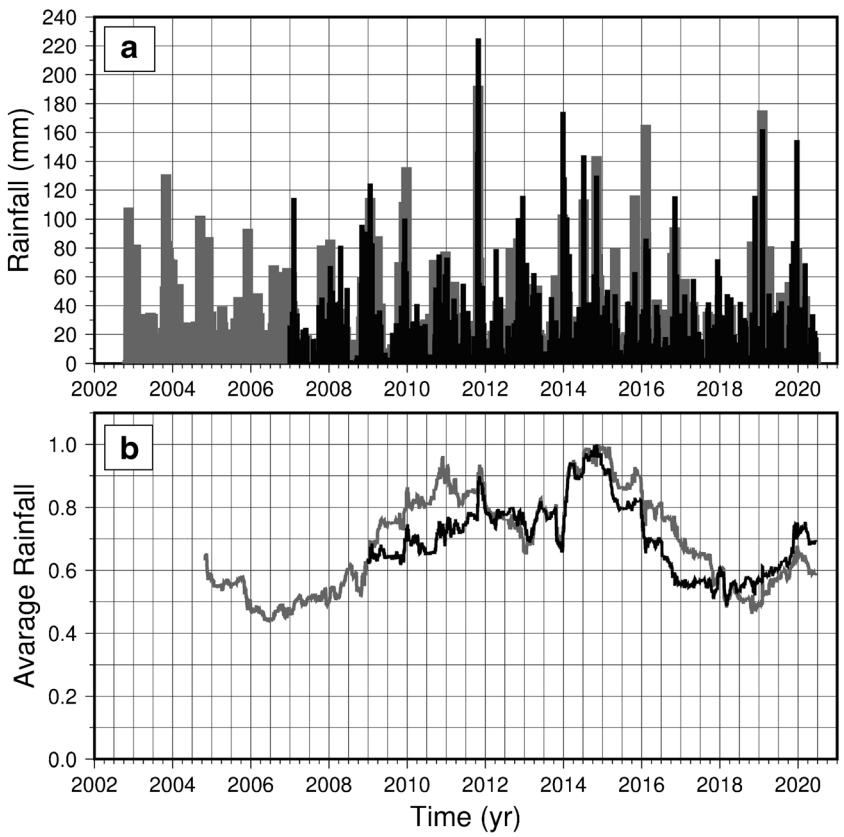

Fig. 3 Rainfall observations. **a** Daily rainfall distribution in millimeters in the Patigno (black bars) and Borgo Val di Taro (gray bars) villages. **b** Normalized average rainfall obtained using a moving window method with size of 730 days and rejecting values derived from windows containing less than 300 days. Black and gray lines represent the values obtained analyzing the Patigno and Borgo Val di Taro daily rainfall time series respectively

Table 3 Velocities (V) and root mean square (RMS) values (in mm/yr and mm respectively) obtained analyzing the daily time series of the North, East, and Vertical coordinates of the sites shown in Fig. 1. PAT1 and PAT2 are the series of Patigno station obtained using RTKLib software with ROGA and ZERI as reference stations, respectively

Code	N	T	North		East		Vertical		Start
			V	RMS	V	RMS	V	RMS	
PAT1	3475	15.0	−36.8 ± 0.6	9.5	21.2 ± 0.6	10.0	−6.0 ± 1.4	25.8	
PAT2	2093	11.4	−37.9 ± 0.6	6.1	21.3 ± 0.4	4.0	−7.3 ± 1.8	19.5	
PATG	3472	15.0	−37.0 ± 0.4	3.7	21.6 ± 0.4	5.8	−6.5 ± 0.8	8.5	2004/01/01
CARG	3192	12.3	−0.3 ± 0.3	1.9	0.2 ± 0.3	1.8	0.4 ± 0.9	5.8	2003/11/06
TREC	3521	11.8	1.2 ± 0.2	2.6	0.02 ± 0.2	2.8	−0.2 ± 0.8	6.0	2003/11/07
ZERI	2645	11.7	−1.0 ± 0.2	2.5	0.6 ± 0.4	4.3	0.0 ± 0.8	6.4	2005/08/24
ROGA	4770	15.0							2003/08/28

PATG is the result of the network approach using the GAMIT software. N is the number of observations in days and T is the working period in years. The uncertainties associated with the velocities have been estimated multiplying the errors by a factor 15. The data related to the first observation are reported in the Start column

InSAR dataset

For this study, we used 200 Sentinel-1A/B Single Look Complex (SLC) SAR images acquired in Interferometric Wide Swath (IW) mode and vertical co-polarization (VV) along the descending track n° 168 (data available from the European Space Agency Open Access Hub, https://scihub.copernicus.eu). The dataset covers a total period of 50 months, from 22 March 2015 to 18 May 2019. The SAR images were cropped to an area of 10 × 10 km centered on the Patigno village and the landslide body. The average incidence angle in the study area is 40.3° from the vertical direction. The pixel spacing is 2.3 m in slant range (perpendicular to orbit) direction and 13.9 m in azimuth (parallel to orbit) direction. The Permanent Scatterer (PS) approach (Ferretti et al. 2001) as implemented in the SARscape software (version 5.5) was used for the time-series analysis. The image acquired on 26 August 2017 was used as master to generate a stack of 199 interferograms that was analyzed following the PS workflow described in detail in Fiaschi et al. (2017 and 2018).

Results

Archival aerial photogrammetry

For each aerial photogrammetric survey, we obtained stereoscopic models with residuals ranging from a few centimeters to the GSD. Table 2 shows the comparison between the coordinates of points located in a presumably stable area outside the landslide body, which provides, in the multi-temporal analysis, the relative co-registration accuracy of the 3D models: the resulting standard deviation is always lower than the larger GSD.

Considering the distribution of the vectors in Fig. 2a and b, characterized by different velocities and planimetric directions, it is possible to divide the landslide body in 3 main sectors: A, Val di Termine; B, Patigno and San Lorenzo; and C, Noce. Taking into account all vectors inside each area, the location of the average vector, the modulus (averaging the size of each measured displacement), the horizontal angle (in respect to the North), and the final velocity were computed together with the standard deviation for the periods 1975–1987 and 1987–2010 (Table 4).

The results of Table 4 are shown in Fig. 2c and d: each velocity vector in the areas A, and B provides the deformation of the landslide body along the direction of the maximum slope (in agreement with the expected movement), with increasing values in the second period (1987–2010). The standard deviation of the directions provides values up to 20°, except for the area C where higher values were obtained: for this area, the size of the final average displacement vector has the same precision of the measure of coordinates related to a generic point located in a stable area (combining the standard deviation in East, North, and Vertical of Table 2).

We analyzed in detail the area of the Patigno village, where the CGNSS site is located. We have calculated the average direction and modulus of the photogrammetric velocity vectors located in a circular area with increasing radius centered on the CGNSS site (Table 5). The differences among the average values obtained with different radius are significantly lower than the associated uncertainties. This result could indicate the absence of important local movements in the area where the CGNSS station is located. Thus, the movements observed by the CGNSS site can be considered representative of the entire area.

GNSS

The local geodetic daily time series components obtained with GAMIT and RTKLib processing are shown in Fig. 4. As it is possible to see, there is an agreement among the time series obtained with the two software with different reference stations; this good correlation is also demonstrated by the agreement between the velocity values reported in Table 3. The GNSS data shows a horizontal movement of about 43 mm/yr in the S-E direction and a loss of surface elevation of few mm/yr (Table 3). The horizontal velocities obtained using the two software with the different reference site (ROGA and ZERI) in the RTKLib processing are in agreement, providing differences less than 1 mm/yr; only the differences between the vertical components are greater than 1 mm/yr. These values could be due to the relative high noise (RMS value greater than 20 mm) in the RTKLib time series and the significant difference among the observed time span, 15 years vs 11 years.

The residual time series, estimated removing the linear trend models from the observation data, show also a good agreement between the GAMIT and RTKLib processing results (Fig. 4d, e and f); these values indicate that the movement of the landslide is characterized by seasonal signals: in particular, the horizontal time

Table 4 Average and RMS of displacement, direction, and velocities of the photogrammetric vectors in the 3 sectors of the Patigno landslide (Fig. 2)

Comparison	Area	N	M (cm)	RMS_M (cm)	θ (°)	RMS_θ (°)	V (mm/yr)
1975–1987	A	49	38	9	157	20	31
	B	83	40	10	151	17	33
	C	33	19	6	30	109	16
1987–2010	A	49	100	9	167	18	43
	B	83	99	9	158	10	43
	C	33	30	14	114	110	13

A (Val di Termine), B (Patigno and San Lorenzo), and C (Noce). The average and root mean square values have been estimated in the 1975–1987 and 1987–2010 periods. N is the number of the vectors available to estimate the statistical values. M and RMS_M are the average and RMS of the displacements in centimeters, respectively. θ and RMS_θ are the average and RMS values of the horizontal direction in degrees and V is the average velocity in mm/yr.

series (North and East) show a signal characterized by a long period. The obtained period and the amplitude of the first five periodic signals are reported in Table 6. The range of the spectrum investigated is from 1 month to the observed time span instead of the half time span as proposed in Cenni et al. (2015). This difference in the procedure have highlighted that the main seasonal signal in the horizontal components of the PATG and PAT1 processing is a multi-annual signal with a period of about 11 years (Table 6). The amplitude and the associated uncertainties of the other signals estimated analyzing the PATG and PAT1 time series indicate that the horizontal movements of the landslide are mainly a combination of multi-annual (11 years) and annual seasonal signals. A multi-annual signal has also been detected in the vertical component of the PATG and PAT1 time series, but the period and amplitude are quite different. The results of the spectral analysis depend strongly on the observation period and on the RMS of the time series analyzed (Table 3). Thus, the high RMS values of RTKLib processing (Table 3) could explain the differences between the PATG and PAT1 vertical time series, and the ranking in the list of the five main seasonal signals. The relatively high difference of observation periods (about 3 years) between PATG-PAT1 and PAT2 could also explain the differences between the periods and the amplitudes of the detected signals (Table 6). The different processing of the same data acquired by the PATG CGNSS station provides time series with a comparable linear trend (Table 3) and seasonal signals (Table 6). This result indicates a horizontal motion of the area where the CGNSS station is located with a mean velocity of about (43 ± 2) mm/yr along the S-E direction (about 150° ± 4°) and a lowering of (−6.5 ± 0.8) mm/yr. These values are in agreement with the ones calculated analyzing the photogrammetric period 1987–2010 in the B zone (Table 4) and in the circular areas around the CGNSS station (Table 5). The velocity values and direction obtained comparing the 1975 and 1987 aerial photogrammetric surveys in the same area are less than the CGNSS values (Tables 4 and 5), which suggests a temporal evolution of the landslide movements between 1975 and 1987 and the last GNSS observation (31 December 2018).

InSAR velocity map

Because the principal displacements of the Patigno landslide occur along the N-S direction (Tables 3 and 4), part of the signal related to this movement cannot be detected through a satellite-based InSAR analysis. The InSAR satellites have, in fact, near-polar orbits and are not sensitive to movements parallel to their orbits and have very little sensitivity (depending on the heading angle) to movements along the N-S direction. Despite this problem, the PS-InSAR analysis of the descending Sentinel-1 images was able to detect movements related to the landslides, probably corresponding mainly to the E-W horizontal component of movement. The mean relative velocity map calculated along the satellite's LOS over the Patigno landslide is presented in Fig. 5. As for the technical limit of the methodology, which rely on highly coherent targets

Table 5 Average velocity of the photogrammetric vectors located in the circular area around the continuous GNSS Patigno station

Comparison	R (m)	N	V (mm/yr)	Average direction
1975–1987	50	4	35 ± 7	148° ± 3°
	100	23	35 ± 7	153° ± 8°
	150	37	34 ± 8	153° ± 8°
	200	51	33 ± 8	153° ± 8°
1987–2010	50	4	46 ± 3	162° ± 3°
	100	23	44 ± 4	162° ± 5°
	150	37	44 ± 4	162° ± 5°
	200	51	43 ± 4	161° ± 6°

R is the search radius in meters, and N is the number of photogrammetric points located at a distance less than the radius from the CGNSS site. The average velocity (V) and horizontal direction are reported in the last two columns together with the RMS values

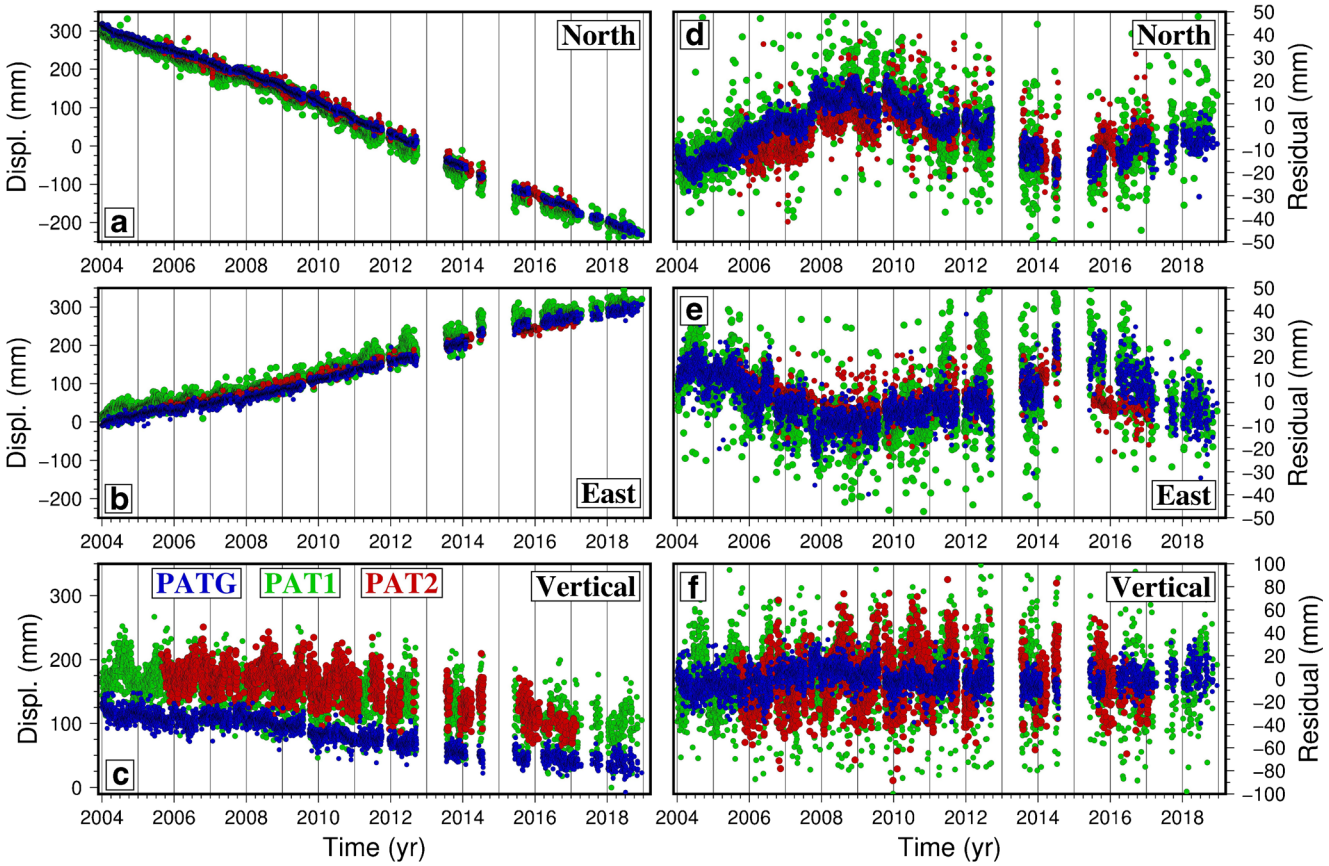

Fig. 4 Daily time series of the local geodetic coordinates (North, East, and Vertical) related to the position of the continuous GNSS Patigno station. The blue points indicate the values obtained using the GAMIT software, the green are the ones obtained by the RTKLib using ROGA site as reference station, and the red are related to the position obtained by the RTKLib using ZERI site as reference station. **a**, **b**, and **c** are the time-series without the outliers, while **d**, **e**, and **f** are the residual time series obtained subtracting the linear model obtained by the velocity values reported in Table 5 to the data

(PS) only, most of the obtained measure points are over the small urban centers of Patigno, Noce, and Val di Termine. In the adopted color scale, considering the descending geometry of acquisition, the positive values (in blue and purple) are the points moving towards the satellite, while the stable points (in green) are the ones with velocities in the ±2 mm/yr range.

If we suppose that the Patigno landslide moves as a rigid block along an inclined plane, the differences among the observed LOS velocities are principally related to the horizontal components of movement. Therefore, the sectors of the landslide where we can observe relatively higher velocities are the ones with larger components of movement in the E-W direction.

The InSAR results show that the PS located in the Patigno village are characterized by values greater than the ones in the other hamlets (Val di Termine and Noce). In particular, it can be noted that the Southern part of the Patigno village presents higher LOS velocities (10–20 mm/yr), which is in agreement with the results obtained analyzing the aerial photogrammetric images acquired in 1987 and 2010. We have also compared the InSAR and the GNSS velocities by projecting the last values to the LOS direction by using the formulas suggested by Hanssen (2001). The obtained values are reported in Table 7, where we have also reported the InSAR rates obtained by averaging the velocities of all PS falling in different circular areas around the CGNSS station. The differences between the velocities of the PATG GNSS LOS and the InSAR average rates are greater than 2 mm/yr. A possible explanation for these differences may be the different observation period, about 15 years for the CGNSS site (Table 3) and 4 years (22 March 2015–19 May 2019) for the SAR observations. For this reason, we have measured the velocity value of the CGNSS station using only the observation period overlapping with the SAR data. The resulting velocities are $V_N = -33.5 \pm 1.2$ mm/yr; $V_E = 12.2 \pm 1.2$ mm/yr; and $V_V = -3.2 \pm 2.0$ mm/yr. The difference between the LOS velocities estimated using only the overlapping period is about 1 mm/yr, less than the RMS associated to the average InSAR values even with the maximum radius considered (200 m, Table 7).

This result validates the InSAR data, and, taking into account the constant LOS velocities of the PS around the CGNSS station and, in general, in the Patigno village, the movements monitored by the GNSS site can be considered as representative of the central-south sector of the Patigno hamlet, as also suggested by the comparison between the aerial photogrammetric vectors and GNSS data discussed in the previous paragraphs. It also highlights the importance of the overlapping period between the available data when a multi-technique monitoring approach is adopted to study a landslide area.

Table 6 Period (in year) and amplitude (in millimeters) of the first five main seasonal signals in the Patigno time series

	N	Period PAT1	Period PAT2	Period PATG	Amplitude PAT1	Amplitude PAT2	Amplitude PATG
North	1	11.1	8.9	11.5	14 ± 3	8 ± 3	13 ± 1
	2	1.1	4.3	1.0	3 ± 3	3 ± 3	2 ± 1
	3	2.4	1.0	2.3	2 ± 3	3 ± 3	1 ± 1
	4	3.1	2.4	3.0	1 ± 3	2 ± 3	1 ± 1
	5	1.6	1.7	0.9	1 ± 3	2 ± 3	1 ± 1
East	1	11.1	8.3	11.5	13 ± 3	6 ± 3	10 ± 1
	2	1.0	4.0	5.4	8 ± 3	2 ± 3	4 ± 1
	3	1.1	2.1	1.1	2 ± 3	1 ± 3	2 ± 1
	4	2.4	2.7	1.0	2 ± 3	1 ± 3	1 ± 1
	5	3.7	1.6	2.9	1 ± 3	1 ± 3	1 ± 1
Vertical	1	1.0	1.0	10.3	14 ± 7	14 ± 6	5 ± 2
	2	13.5	5.6	1.0	5 ± 7	6 ± 6	4 ± 2
	3	1.2	3.4	1.2	3 ± 7	5 ± 6	3 ± 2
	4	0.7	2.2	0.9	3 ± 7	3 ± 6	2 ± 2
	5	0.6	1.6	0.6	1 ± 7	3 ± 6	2 ± 2

These values have been obtained analyzing with a nonlinear least squares technique (Lomb (1976)–Scargle (1982) approach) the residual daily time series of the position components. The spectrum of each component has been analyzed in order to estimate the period of the five (statistically meaningful) main signals in the interval between 1 month and the observation period. *N* represents the magnitude of the signal in the power spectrum, i.e., the signal with the highest power in the spectrum is the first (*N*=1) signal

Discussions

Rainfall

The kinematic of the Patigno landslide is mainly driven by the hydrology of the site (Baldi et al. 2008). In order to better understand this hydrological control on the landslide movement, we have analyzed with an average moving window method the daily rainfall time series measured by the pluviometric stations located at Patigno and Borgo Val di Taro. The normalized average moving window values obtained using a window of 730 days and rejecting the values derived from windows shorter than 300 days are presented in Fig.3b. The average moving window is a low pass filter that attenuates signals with frequencies higher than the window size, and we have assigned the average values to the date of the last day in the window; therefore, the obtained values represent the rainfall distribution before the data observed in the figures. The similarity between the rainfall datasets increases if we consider the average time series shown in Fig. 3b, with a Pearson's correlation coefficient of about 0.8 and vanishing time lag. It can be also noted that the average time series show a multi-seasonal signal with a period probably greater than the available rainfall time span and an annual signal with a rainy season from autumn to winter. The good agreement between the rainfall distribution observed in the Patigno and Borgo Val di Taro villages demonstrates the possibility to compare the second dataset, characterized by the longest time span, with the GNSS time series and to evaluate how the rainfall distribution drives the landslide movements.

Photogrammetry

The kinematic patterns obtained comparing the 1975–1987 and 1987–2010 photogrammetric surveys clearly indicate that the landslide area can be subdivided in three main sectors with different average velocities values and different directions of the displacement vectors (Table 4 and Fig. 2c and d , Fig. 6a and b). Sectors A and B present similar kinematic behavior during the monitored periods (1975–1987 and 1987–2010). The different direction of the movement and the low velocity rates observed in C (Table 4 and Figs. 2, 6) are probably representative of the landslide toe, where the sliding movements slow down and where the scatter of the displacement direction increases also due to the gentle slope of this area (Fig. 2) and the erosion of the Gordana river (Fig. 1). A relatively low rates of C has also been observed in the InSAR LOS velocity map of Fig. 5, even if the SAR images are more recent than the aerial photogrammetric surveys.

The photogrammetric analysis indicates that the velocity increases in the period 1987–2010 in respect to 1975–1987, and the strain rate fields (Fig. 6c and d) suggest how this acceleration has modified the deformation pattern in the landslide area. It can be noted that the western side of sector A is characterized by a contraction strain pattern (red area in Fig. 6c and d) probably related to the supply material from the eastern and/or upper part of the landslide. The effects of this contraction increased in the period 1987–2010, also in the western side of B (Fig. 6d). The concurrent increasing of extension pattern in C and the contraction in the western side of B suggests that the supply material generated by the acceleration of the landslide in the upper part was partially eroded by the Gordana river in the southern boundary of C and partially accumulated in the western side of A and B. The area at the CGNSS site (central part of sector B) is characterized by lower values of dilatation (Fig. 6c and d), with an increase of extensional pattern in the period 1987–2010. The orientation and

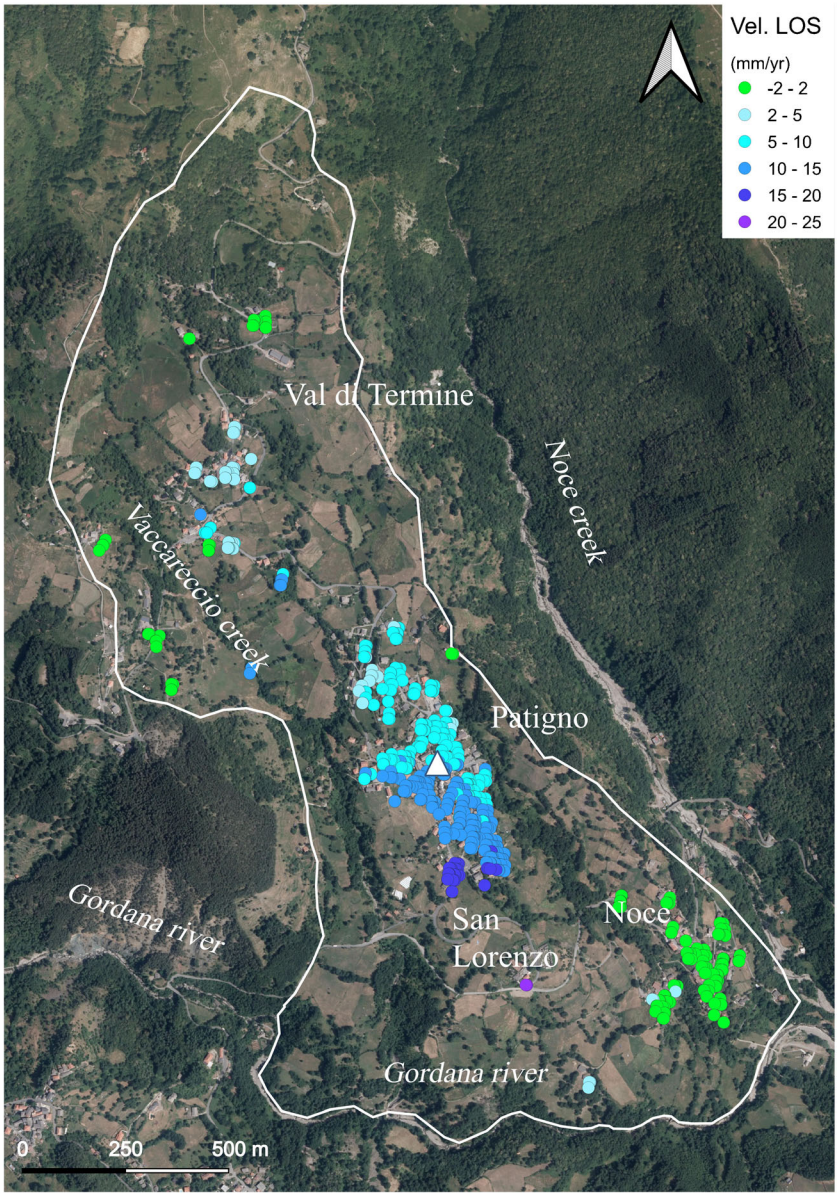

Fig. 5 Line of sight velocity map derived from the PS InSAR analysis of Sentinel-1 images from March 2015 to May 2019 over the study area. The white triangle indicates the position of the CGNSS station. The blue and purple positive values indicates the points moving towards the Sentinel-1 satellite, while the green indicates stable points

size of the principal axes could suggest that the Patigno village represents the upper boundary of the extensional sector of the landslide.

The strain values estimated using the archival aerial photogrammetric surveys are about two order of magnitude greater than the ones of the tectonic movements in the Italian peninsula (maximum strain rate ~10^{-7}/yr) (e.g., Anderlini et al. 2016; Esposito et al. 2020; Cenni et al. 2012). This suggests that the buildings located in the landslide area could be subjected to stress analogous to a seismic event. For example, we can estimate the stress due to the strain rate pattern in the landslide area with a simple uniaxial elastic model where the relation between stress (σ) and strain (ε) is driven by the Young's modulus E ($\sigma = E\ \varepsilon$). Considering an average value of 70 GPa for the Young's modulus (typical for the crust rocks) and a strain rate of about 10^{-5} 1/year, we obtain a stress of few bars (~10^5 Pa). This value is comparable with the changing Coulomb stress in the area closest to the main seismic events in the Italian peninsula (e.g., Cheloni et al. 2016; Serpelloni et al. 2012). The stress variation in the landslide area occurs in a period (1 year) greater than a seismic event (few seconds): this difference reduces considerably the hazard of the stress variation. The estimated strain rate field shown in Fig. 6c and d can provide useful information about the area where the buildings are subjected to relatively high deformations. In particular, the central zone of the B sector, where the highest velocity values are detected and the deformation regime changes from

Table 7 Average PS InSAR LOS velocity around the continuous GNSS Patigno station

R (m)	*N*	*V* (mm/yr)	RMS (mm/yr)
10	2	10	0.3
25	10	10	1.1
50	29	10	1.3
100	109	9	1.8
150	196	10	1.8
200	258	10	1.8
PATG		13	
PATG-2015		9	

R is the search radius in meters. *N* is the number of permanent scatters located in each circle. The average velocity (*V*) and the root mean square values (RMS) were estimated using the PS near the CGNSS site. The PATG and PATG-2015 are the velocities of the CGNSS site obtained along the LOS of the Sentinel-1 satellite using the following parameters: Incidence angle = 40.31° and azimuth angle = −80.73°. The PATG-2015 value has been calculated using the velocities computed with only the GNSS time series overlapping to the InSAR data (starting on 22 March 2015). The obtained velocity values of the three components are: $V_N = (-33.5 \pm 1.2)$ mm/yr; $V_E = (12.2 \pm 1.2)$ mm/yr; and $V_V = (-3.2 \pm 2.0)$ mm/yr

compression to extension, could be identified as the area where the sliding of the landslide could damage the buildings more seriously, as also suggested by Del Soldato et al. (2019).

The scattering observed in the aerial photogrammetric vectors (Fig. 2) and InSAR velocities (Fig. 5) in the landslide area suggests the need to first investigate the similarities of the values closest to the CGNSS site prior to compare the results of the two techniques in the whole area. The average values of the modulus and direction of the horizontal photogrammetric velocities reported in Table 4, calculated considering a circular area around the position of the CGNSS site, suggest that the movement of the area inside to the Patigno village is characterized by a uniform motion, without particular local effects. The results reported in Table 3 indicate the absence of significant differences between the modulus and direction of the velocity values obtained using the different processing of the GNSS data. The horizontal GNSS velocity (43 ± 2) mm/yr and direction (150°± 4°) of the Patigno site are in agreement with the ones calculated in the 1987–2010 photogrammetric period in sector B (Tables 4 and 5). This result is probably given by the partial overlap between the two observation periods. The kinematic pattern estimated in 1975–1987 is characterized by values of velocity less than the subsequent period (1987–2010) and the GNSS values, which indicates a temporal variability of the landslide movements.

CGNSS

The temporal variability of the kinematic pattern can be drawn by comparing the GNSS velocity projected to the LOS and the InSAR results (Table 7). In fact, the reported values are in agreement especially when the observation period is completely overlapped. Previous studies (Baldi et al. 2008; Del Soldato et al. 2019) have also pointed out such temporal variation of the sliding velocity. Baldi et al. (2008) have estimated a seasonal variation of the horizontal sliding velocity between 30 and 60 mm/yr analyzing the weekly time series with a "mobile velocity window" method. By obtaining a positive correlation between the CGNSS data and the rainfall distribution, they suggest that the creep of the landslide is influenced by hydrological factors. We have analyzed the daily CGNSS time series of PATG site obtained with the three different processing and using a similar "mobile velocity method". Figure 7 shows the four time series (three local geodetic components and the horizontal displacement) obtained using a window of 730 days and rejecting values derived from windows containing less than 300 days. It can be noted as the "velocity moving window" time series (VMW) of the horizontal components (North, East, and Horizontal) calculated with the three different processing (GAMIT and RTKLib) are in good agreement, as also attested by the Pearson's correlation coefficient (Fig. 7). The VMW of the vertical components obtained with RTKLib software are also in good agreement, but the seasonal signals are quite different in respect to the ones obtained with the GAMIT processing (Fig. 7c). These significant disagreements are probably due to the poor accuracy of the GNSS technique on the vertical component in respect to the horizontal direction. In particular, the high correlation between the noise on the vertical GNSS component and the accuracy of the parameters of the models adopted during the processing, could introduce in the time series not negligible signals (e.g., Klos et al. 2019), which can be detected by a moving window analysis and can introduce a high noise and spurious signals in the VMW time series.

We have also investigated a possible correlation between the changes in the VMW time series and the rainfall distribution in the Lunigiana area. The maximum values of the Pearson correlation coefficient estimated with a time lag from −800 to 800 days are reported in Table 8: the maximum correlation between the horizontal velocity and the rainfall distribution, with a coefficient of about 0.9, was obtained using the processing with the GAMIT software (PATG code in Table 8). The values of the vertical component seem to be less correlated with the rainfall: however, the PATG solution indicates a good agreement with the rainfall distribution with a lag (168 days) slightly different than the horizontal component (120 days). In agreement with the present results, previous studies (Baldi et al. 2008) have detected seasonal variations in the horizontal velocity controlled by the hydrological history. The daily moving window and the increasing of the observation period have provided a more precise estimation of the time lag (about 120 days) between the rainfall and the increasing of the sliding velocity. This late response of the landslide to the rainfall distribution could be due to the slow infiltration of rainwater through the clayey soils of the landslide body and consequent rise in interstitial pore-water pressure, as suggested by Baldi et al. (2008). Other authors (Federici et al. 2002, Stucchi et al. 2014), analyzing the displacements recorded in the boreholes distributed on the Patigno slope, and the results of a P-wave high-resolution reflection seismic survey, have suggested that the landslide displacements involve rock volumes up to 50 m depth. The deeper slow-rate displacements observed in the boreholes and the laboratory tests have suggested an active visco-plastic deformation in the layer composed by inhomogeneous material (boulders, gravel, and coarse sand) underlying the superficial highly fractured argillites and limestone layer. The boundary between the densely fractured rocks layer and the undisturbed bedrock could be the limit where the increasing of water pressure induces a reduction of the internal shear strength and facilitates the sliding.

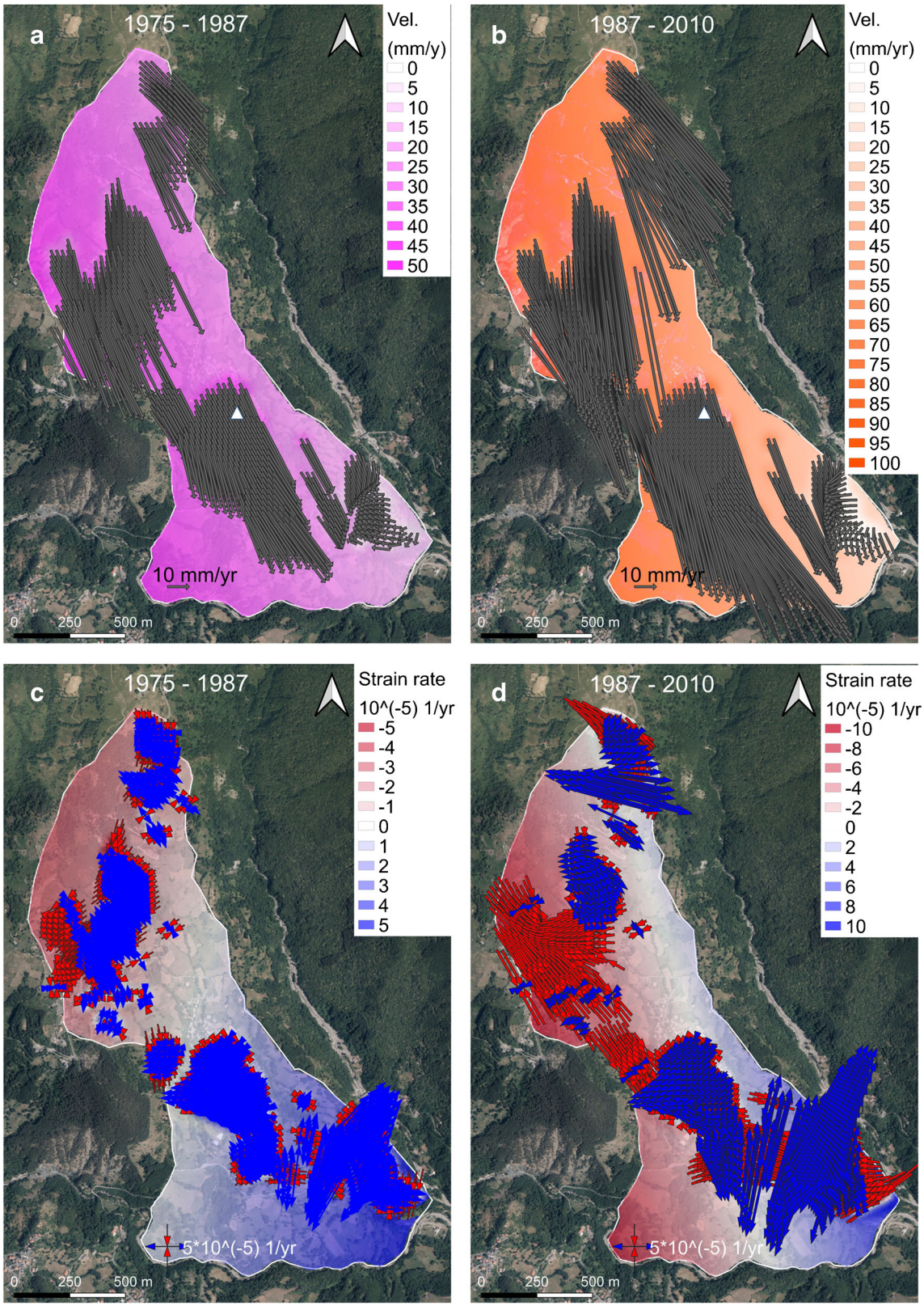

Fig. 6 Interpolated kinematic field deformation pattern. **a** and **b** Interpolated horizontal velocity field obtained on a regular grid (spacing of 25 meters) for the two analyzed periods. The gray arrows show the interpolated horizontal velocities where it was possible to estimate the values. The modulus of the interpolated horizontal velocity vectors is also displayed by a graduated color scale reported in the upright corner of the figures. **c** and **d** Trace of the strain rate matrix or dilation strain rate (positive is the blue extension, negative is the red contraction) for the same periods. Superimposed are the orientations and relative size of the main axes: red vectors are negative (contraction) and blue are positive (extension). The interpolated values are estimated by a decay factor of 200 m.

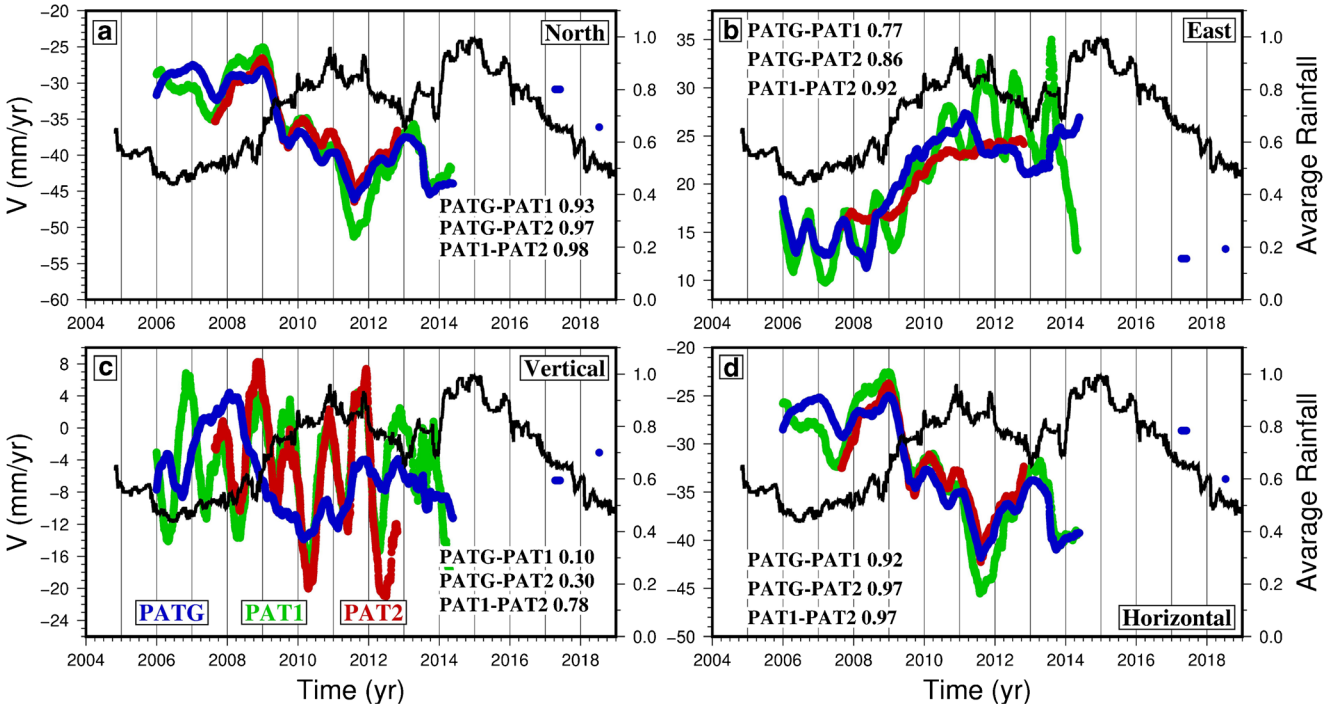

Fig. 7 "Instantaneous" landslide velocity detected using the "moving velocity window" (VMW) method with a size of 730 days and rejecting values derived from windows containing less than 300 days. We have analyzed the time series shown in Fig. 4a, b, and c: they represent the local geodetic coordinates of the Patigno CGNSS site (**a** North, **b** East, and **c** Vertical); **d** is the velocity time-series of the Horizontal component obtained combining the North and East coordinates. The blue points have been obtained analyzing the GAMIT processing results (PATG), while the red and green points have been obtained analyzing the RTKLib processing results using ZERI (PAT2) and ROGA (PAT1) as reference stations, respectively. The black points are the normalized average moving window rainfall values related to the data (collected in the Borgo Val di Taro site, Fig. 1, and obtained using the same size of the window). The Pearson's correlation coefficients between the three GNSS time-series are also reported

A rigid block sliding downwards along an inclined plane could be a simple model that can be used in order to reproduce the displacements of the Patigno landslide; from the simple formulas of the inclined plane, we can estimate the slope angle of the sliding boundary layer using the horizontal and vertical components of the velocity obtained with the GNSS observation reported in Table 3. We have obtained a slope angle of about 9°, a value similar to the slope of the ground estimated by analyzing the 1975 aerial photogrammetric survey (about 10°, Baldi et al. 2008). This result indicates that the deep boundary in the sector of the CGNSS station is parallel to the terrain surface. Furthermore, the refraction seismic surveys and electrical resistivity profiles (Stucchi et al. 2014 and Tuscany internal report 2005) carried out in the same sector of the landslide indicate that the boundary between the coarse landslide material and the undisturbed bedrock is characterized by a slope angle like the ground.

Integrated monitoring

The integrated use of data generated with different techniques has the main advantage of producing more reliable results, by overcoming the limitations of each technique, namely, the resolution for the GNSS, the long-term availability of archival data (for GNSS and InSAR), the accuracy (for aerial photogrammetry), and the type of acquired information (only LOS for InSAR).

However, the comparison of results obtained using different approaches often introduces a problem related to the selection of a common reference frame, which can potentially introduce a bias in the obtained values. We have solved the reference frame issue using the GNSS permanent station as a reference and estimating the GNSS velocity only using the time series overlapping the InSAR observations and the aerial photogrammetric surveys closest to the GNSS data (Table 7).

The proposed integrated monitoring approach gives the possibility to monitor the evolution of the Patigno landslide in the last

Table 8 Pearson correlation coefficients between the GNSS VMW time series and the rainfall average moving windows shown in Fig. 7

	North	East	Horizontal	Vertical
PATG	−0.90 (118)	0.92 (57)	−0.89 (120)	−0.7 (168)
PAT1	−0.84 (255)	0.86 (352)	−0.81 (206)	0.1 (-800)
PAT2	−0.86 (206)	0.96 (281)	−0.84 (205)	−0.34 (759)

The first value in the cell is the maximum value of the Pearson cross-correlation coefficient and the values in the brackets correspond to the time lag in days. The time lag varies between -800 and 800 days. Positive values of the time lag indicate a positive shift in the time scale of the rainfall time series, i.e., the rainfall anticipates the GNSS velocity time series

44 years using data originally acquired for other purposes, such as the cartographic mapping with aerial photogrammetric surveys, and the tectonic monitoring of the Lunigiana graben with the GNSS sites.

Conclusions

In this work, we adopted an approach based on the integration of different type of techniques, the use of nonconventional software and different data processing approaches, to monitor the evolution of the Patigno landslide. The results obtained by comparing the GAMIT and RTKLib processing have highlighted that the use of open-source software does not represent a limit to estimate the average horizontal sliding rate of the landslide, providing uncertainties less than 2 mm/yr. Moreover, the use of the open-source software allowed us to estimate the main characteristics of the seasonal variations on the horizontal components related to the rainfall distribution. Significant differences between GAMIT and RTKLib can be observed in the periodic signals of the vertical component, but the estimated velocity values are in agreement. Therefore, an open-source software such as RTKLib can be adopted by the local authorities to monitor the main movements of deep-seated gravitational slope deformation such as the Patigno landslide. The GNSS results have also demonstrated that the main changes of the landslide displacements can be detected using a reference site located at a distance of some tens of km. Possible hydrological triggering mechanisms have been studied comparing the VMW values with the rainfall average moving window values, which showed an acceleration of the sliding movements after about 3–4 months of a period of strong rainfall. This information could be useful to the local authorities to develop strategies for risk mitigation after a strong rainfall period.

The multi-temporal archival aerial photographs have documented the Patigno landslide activity in the 1975–2010 period, while the SAR images allowed to extend the observation period until 2019, which provides a total monitoring period of about 44 years. The results obtained through the archival multi-temporal digital photogrammetry indicate that the kinematic pattern of the landslide can be divided in three sectors characterized by different velocity values. Similar results were also obtained through the processing of the 2015–2019 InSAR data. The photogrammetric approach, confirmed by the InSAR data even if referring to different periods, showed that the sector B, where the Patigno hamlet is located, is the area where the highest velocities and deformations are recorded and where the strain rate regime changes from compression to extension. For these reasons, this portion of the landslide can be assumed as the most dangerous, as the movements of the ground could cause serious damages to the buildings.

The upper landslide sector and Noce hamlet, at the toe of the landslide, are also characterized by an important extensional pattern. In the Noce hamlet, the results of the photogrammetric analysis are limited due to the resolution of the technique: therefore, in this area higher resolution data are needed in order to obtain more information about the kinematic and deformation patterns. The south area of the Patigno village and San Lorenzo hamlet, located in the central-south sector of the landslide, are the zones characterized by the highest InSAR LOS velocity values: since no substantial differences emerged with the photogrammetric vectors compared to the Patigno village results, the increase in deformation in this area could be the result of recent phenomena, which increase the risk in this area.

This study confirms that a multi-technique approach can be used as a valuable tool to better understand the landslide kinematics and provides local authorities with the information needed to better plan the risk mitigation strategies.

Acknowledgements

The authors would like to thank Prof. Enzo Mantovani, Prof. Dario Albarello, and Dr. Marcello Viti of Department of Physical Sciences, Earth and Environment of the University of Siena for providing the GNSS data. The authors would also like to thank Dr. Massimo Baglione, Dr. Vittorio D'Intinosante, and Dr. Pierangelo Fabbroni of the Servizio Sismico-Regione Toscana for providing the archival aerial photogrammetric surveys of 2010 and 2013. Several figures (Fig. 1 inset, 3, 4, 7) were generated with the Generic Mapping Tools (Wessel et al. 2013). The authors deeply thank the reviewers and the editor for their constructive and helpful comments.

Author contribution

Nicola Cenni—GNSS data processing, multi-technique approach, data interpretation, and writing of the manuscript

Simone Fiaschi—InSAR data processing, data interpretation, and writing of the manuscript

Massimo Fabris—Aerial photogrammetric data processing, data interpretation, and writing of the manuscript

Declarations

Competing interests The authors declare no competing interests.

References

Achilli V, Carrubba P, Fabris M, Menin A, Pavanello P (2015) An archival geomatics approach in the study of a landslide. Appl Geom. 7(4):263–273. https://doi.org/10.1007/s12518-015-0153-4

Anderlini L, Serpelloni E, and Belardinelli ME (2016) Creep and locking of a low-angle normal fault: Insights from the Altotiberina fault in the Northern Apennines (Italy). Geophys Res Lett 43(9)4321–4329. https://doi.org/10.1002/2016GL068604

Baldi P, Cenni N, Fabris M, Zanutta A (2008) Kinematics of a landslide derived from archival photogrammetry and GPS data. Geomorphology 102(3–4):435–444. https://doi.org/10.1016/j.geomorph.2008.04.027

Bortolotti V, Fazzuoli M, Pandeli E, Principi G, Babbini A, Corti S (2001) Geology of central and eastern Elba Island, Italy. Ofioliti 26:97–150

Bos MS, Fernandes RMS, Williams SDP, Bastos L (2013) Fast error analysis of continuous GNSS observations with missing data. J Geod 87(4):351–360. https://doi.org/10.1007/s00190-012-0605-0

Calò F, Ardizzone F, Castaldo R, Lollino P, Tizzani P, Guzzetti F, Lanari R, Angeli MG, Pontoni F, Manunta M (2014) Enhanced landslide investigations through advanced DInSAR techniques: the Ivancich case study, Assisi, Italy. Remote Sens Environ 142:69–82. https://doi.org/10.1016/j.rse.2013.11.003

Carmignani L, Decandia FA, Disperati L, Fantozzi PL, Kligfield R, Lazzarotto A, Liotta D, Meccheri M (2001) Inner northern Apennines. In: Vai G, Martini P (eds) Anatomy of an orogen: the Apennines and adjacent Mediterranean Basins. Kluwer, Academic Publishers, Dordrecht, pp 197–214

Cenni N, Mantovani E, Baldi P, Viti M (2012) Present kinematics of Central and Northern Italy from continuous GPS measurements. J Geodyn 58:62–72

Cenni N, Viti M, Baldi P, Mantovani E, Bacchetti M, Vannucchi A (2013) Present vertical movements in central and northern Italy from GPS data: possible role of natural and anthropogenic causes. J Geodyn 71:74–85

Cenni N, Viti M, Mantovani E (2015) Space geodetic data (GPS) and earthquake forecasting: examples from the Italian geodetic network. Boll Geofis Teor Appl 56(2):129–150. https://doi.org/10.4430/bgta0139

Cheloni D, Giuliani R, D'Agostino N, Mattone M, Bonano M, Fornaro G, Lanari R, Reali D, Atzori S (2016) New insights into fault activation and stress transfer between en echelon thrusts: the 2012 Emilia, Northern Italy, earthquake sequence. J Geophys Res Solid Earth 121(6):4742–4766. https://doi.org/10.1002/2016JB012823

Cina A, Piras M (2015) Performance of low-cost GNSS receiver for landslides monitoring: test and results, Geomatics. Nat Hazards and Risk 6(5-7):497–514. https://doi.org/10.1080/19475705.2014.889046

Colesanti C, Ferretti A, Prati C, Rocca F (2003) Monitoring landslides and tectonic motions with the Permanent Scatterers Technique. Eng Geol 68:3–14

Corominas J, Moya J, Lloret A, Gili J, Angeli M, Pasuto A, Silvano S (2000) Measurement of landslide displacements using a wire extensometer. Eng Geol 55:149–166

Cotecchia V, Grassi D, Merenda L (1995) Fragilità dell'area urbana occidentale di Ancona dovuta a movimenti di massa profondi e superficiali ripetutisi nel 1982. Geol Appl Idrogeol 30:633–657

Del Soldato M, Solari L, Poggi F, Raspini F, Tomás R, Fanti R, Casagli N (2019) Landslide-induced damage probability estimation coupling InSAR and field survey data by fragility curves. Remote Sens 11(12):1486. https://doi.org/10.3390/rs11121486

Di Naccio D, Boncio P, Brozzetti F, Pazzaglia FJ, Lavecchia G (2013) Morphotectonic analysis of the Lunigiana and Garfagnana grabens (northern Apennines, Italy): Implications for active normal faulting. Geomorphology 201:293–311. https://doi.org/10.1016/j.geomorph.2013.07.003

Dreyfus D, Rathjea EM, Jibson RW (2013) The influence of different simplified sliding-block models and inputparameters on regional predictions of seismic landslides triggered by the Northridge earthquake. Eng Geol 163:41–54. https://doi.org/10.1016/j.enggeo.2013.05.015

Esposito A, Galvani A, Sepe V, Atzori S, Brandi G, Cubellis E, De Martino P, Dolce M, Massucci A, Obrizzo F, Pietrantonio G, Riguzzi F, Tammaro U (2020) Concurrent deformation processes in the Matese massif area (Central-Southern Apennines, Italy). Tectonophysics 774:228234. https://doi.org/10.1016/j.tecto.2019.228234

Fabris M (2019) Coastline evolution of the Po River Delta (Italy) by archival multi-temporal digital photogrammetry. Geom, Nat Hazards and Risk 10(1):1007–1027. https://doi.org/10.1080/19475705.2018.1561528

Fabris M, Pesci A (2005) Automated DEM extraction in digital aerial photogrammetry: precisions and validation for mass movement monitoring. Ann Geophys 48(6):57–72. https://doi.org/10.4401/ag-3247

Fabris M, Baldi P, Anzidei M, Pesci A, Bortoluzzi G, Aliani S (2010) High resolution topographic model of Panarea island by fusion of photogrammetric, lidar and bathymetric Digital Terrain Models. Photogramm Rec 25(132):382–401. https://doi.org/10.1111/j.1477-9730.2010.00600.x

Fanti R, Gigli G, Lombardi L, Tapete D, Canuti P (2013) Terrestrial laser scanning for rockfall stability analysis in the cultural heritage site of Pitigliano (Italy). Landslides 10(4):409–420. https://doi.org/10.1007/s10346-012-0329-5

Federici P, Puccinelli A, Chelli A, D'Amato Avanzi G, Ribolini A, Verani M (2000) La grande frana di Patigno di Zeri (Massa-Carrara). Memorie della Accademia Lunigianese di Scienze Giovanni Capellini. Scienze Naturali Fisiche e Matematiche 70:31–41

Federici PR, Puccinelli A, Chelli A, D'Amato AG, Ribolini A, Verani M (2002) The large landslide of Patigno (Northern Apennines, Italy): geological, geomorphological and geognostic integrated analysis. In: Rybar J, Stemberg J, Wagner P (eds) Landslides. Swets and Zeitlinger, Lisse, pp 547–552

Feng ZY, Huang HY, Chen SC (2020) Analysis of the characteristics of seismic and acoustic signals produced by a dam failure and slope erosion test. Landslides 17(7):1605–1618. https://doi.org/10.1007/s10346-020-01390-x

Ferretti A, Prati C, Rocca F (2001) Permanent scatterers in SAR interferometry. IEEE Trans Geosci Remote Sens 39(1):8–20

Fiaschi S, Mantovani M, Frigerio S, Pasuto A, Floris M (2017) Testing the potential of Sentinel-1 TOPS interferometry for the detection and monitoring of landslides at local scale, Veneto Region, Italy. Environ Earth Sci 76(492). https://doi.org/10.1007/s12665-017-6827-y

Fiaschi S, Fabris M, Floris M, Achilli V (2018) Estimation of land subsidence in deltaic areas through differential SAR interferometry: the Po River Delta case study (NE Italy). Int J Remote Sens 39(23):8724–8745. https://doi.org/10.1080/01431161.2018.1490977

Frigerio S, Schenato L, Bossi G, Cavalli M, Mantovani M, Marcato G, Pasuto A (2014) A web-based platform for automatic and continuous landslide monitoring: the Rotolon (Eastern Italian Alps) case study. Comput Geosci 63:96–105. https://doi.org/10.1016/j.cageo.2013.10.015

Frodella W, Ciampalini A, Gigli G, Lombardi L, Raspini F, Nocentini M, Scardigli C, Casagli N (2016) Synergic use of satellite and ground based remote sensing methods for monitoring the San Leo rock cliff (Northern Italy). Geomorphology 264:80–94

Glansch J, Heunecke O, Schuhbäck S (2009) Monitoring the Hornbergl landslide using a recently developed low cost GNSS sensor network. Jof Applied Geodesy 3:179–1926. https://doi.org/10.1515/JAG.2009.019

Hanssen RF (2001) Radar interferometry: data interpretation and error analysis. Springer Science & Business Media: Dordrecht, Netherland

He X, Montillet JP, Fernandes R, Bos M, Yu K, Hua X, Jiang W (2017) Review of current GPS methodologies for producing accurate time series and their error sources. J Geodyn 106(February):12–29. https://doi.org/10.1016/j.jog.2017.01.004

Herring, T.A., King, R.W., Floyd, M.A. & McClusky, S.C., 2018. GAMIT Reference Manual, GPS Analysis at MIT, Release 10.7. Department of Earth, Atmospheric and Planetary Sciences, Massachusset Institute of Technology, Cambridge

Inventario Fenomeni Franosi Italia – ISPRA 2020 http://www.isprambiente.gov.it/it/progetti/suolo-e-territorio-1/iffi-inventario-dei-fenomeni-franosi-in-italia. accessed on 6 August, 2020

ISIDe Working Group. (2007). Italian Seismological Instrumental and Parametric Database (ISIDe). Istituto Nazionale di Geofisica e Vulcanologia (INGV) https://doi.org/10.13127/ISIDE

Kean, JW, Coe JA, Coviello V, Smith JB, Mccoy, SW, Arattano M, (2015). Estimating rates of debris flow entrainment from ground vibrations. https://doi.org/10.1002/2015GL064811, Estimating rates of debris flow entrainment from ground vibrations.

Klos A, Bos M S, Fernandes R M S, Bogusz J (2019) Noise-dependent adaption of the wiener filter for the GPS position time series. Math Geosci 51(1):53–73. https://doi.org/10.1007/s11004-018-9760-z

Komac M, Holley R, Mahapatra P, van der Marel H, Bavec M (2015) Coupling of GPS/GNSS and radar interferometric data for a 3D surface displacement monitoring of landslides. Landslides 12(2):241–257. https://doi.org/10.1007/s10346-014-0482-0

Liu D, Leng X, Wei F, Zhang S, Hong Y (2018) Visualized localization and tracking of debris flow movement based on infrasound monitoring. Landslides 15(5):879–893. https://doi.org/10.1007/s10346-017-0898-4

Manconi A, Picozzi M, Coviello V, De Santis F, Elia L (2016) Real-time detection, location, and characterization of rockslides using broadband regional seismic networks. Geophys Res Lett 43(13):6960–6967. https://doi.org/10.1002/2016GL069572

Mao A, Harrison CGA, Dixon TH (1999) Noise in GPS coordinate time series. J Geophys Res 104(B2):2797–2816. https://doi.org/10.1029/1998JB900033

Pesci A, Baldi P, Bedin A, Casula G, Cenni N, Fabris M, Mora P, Bacchetti M (2004) Digital elevation models for landslide evolution monitoring: Application on two areas located in the Reno River Valley (Italy). Ann Geophys 47(4)

Pesci A, Teza G, Casula G (2009) Improving strain rate estimation from velocity data of non-permanent GPS stations: The central Apennine study case (Italy). GPS Solutions 13(4):249–261. https://doi.org/10.1007/s10291-009-0118-3

Raiti R, Signanini P, Torrese P, Sammartino P (2006) Il metodo della ricollocazione nella risoluzione di problematiche geologicoambientali: Il caso di Zeri (Massa-Carrara). G Di Geol Appl 3:213–220

Refice A, Campolongo D (2002) Probabilistic modeling of uncertainties in earthquake-induced landslide hazard assessment. Comput Geosci 28(6):735–749. https://doi.org/10.1016/S0098-3004(01)00104-2

Rovida A, Locati M, Camassi R, Lolli B, Gasperini P (2020) The Italian earthquake catalogue CPTI15. Bull Earthq Eng 18(7):2953–2984. https://doi.org/10.1007/s10518-020-00818-y

Serpelloni E, Anderlini L, Belardinelli ME (2012) Fault geometry, coseismic-slip distribution and Coulomb stress change associated with the 2009 April 6, M w 6.3, L'Aquila earthquake from inversion of GPS displacements. Geophys J Int 188(2):473–489. https://doi.org/10.1111/j.1365-246X.2011.05279.x

Stucchi E, Ribolini A, Anfuso A (2014) High-resolution reflection seismic survey at the Patigno landslide, Northern Apennines, Italy. Near Surf Geophys 12(4):559–571. https://doi.org/10.3997/1873-0604.2013036

Takasu, T. (2013). RTKLIB: An open source program package for GNSS positioning. Software and documentation available at: http://www.rtklib.com, accessed on 6 August, 2020

Teza G, Pesci A, Galgaro A (2008) Grid_strain and grid_strain3: Software packages for strain field computation in 2D and 3D environments. Comput Geosci 34(9):1142–1153. https://doi.org/10.1016/j.cageo.2007.07.006

Umar Z, Pradhan B, Ahmad A, Neamah JM, Shafapour TM (2014) Earthquake induced landslide susceptibility mapping using an integrated ensemble frequency ratio and logistic regression models in West Sumatera Province, Indonesia. Catena 118:124–135. https://doi.org/10.1016/j.catena.2014.02.005

Wang W, Zhao B, Wang Q, Yang S (2012) Noise analysis of continuous GPS coordinate time series for CMONOC. Adv Space Res 49(5):943–956. https://doi.org/10.1016/j.asr.2011.11.032

Wessel P, Smith WHF, Scharroo R, Luis J, Wobbe F (2013) Generic mapping tools: improved version released, EOS Trans. AGU 94(45):409–410. https://doi.org/10.1002/2013EO450001

Yan Y, Cui Y, Tian X, Hu S, Guo J, Wang Z, Yin S, Liao L (2020) Seismic signal recognition and interpretation of the 2019 "7.23" Shuicheng landslide by seismogram stations. Landslides 17(5):1191–1206. https://doi.org/10.1007/s10346-020-01358-x

Zhang Y, Tang H, Li C, Lu G, Cai Y, Zhang J, Tan F (2018) Design and testing of a flexible inclinometer probe for model tests of landslide deep displacement measurement. Sensors 18:224

N. Cenni (✉)
Department of Geosciences,
University of Padova,
Padua, Italy
Email: nicola.cenni@unipd.it

S. Fiaschi
UCD School of Earth Sciences,
University College Dublin,
Dublin, Ireland

M. Fabris
Department of Civil, Environmental and Architectural Engineering,
University of Padova,
Padua, Italy